



HAL
open science

Heat transfer enhancement of a natural convection flow in an enclosure submitted to a small extent thermal disturbance: Influence of location and frequency

Paul Chorin, Florian Moreau, Didier Saury

► To cite this version:

Paul Chorin, Florian Moreau, Didier Saury. Heat transfer enhancement of a natural convection flow in an enclosure submitted to a small extent thermal disturbance: Influence of location and frequency. International Journal of Thermal Sciences, 2020, pp.106711. 10.1016/j.ijthermalsci.2020.106711 . hal-03029811

HAL Id: hal-03029811

<https://hal.science/hal-03029811>

Submitted on 3 Feb 2023

HAL is a multi-disciplinary open access archive for the deposit and dissemination of scientific research documents, whether they are published or not. The documents may come from teaching and research institutions in France or abroad, or from public or private research centers.

L'archive ouverte pluridisciplinaire **HAL**, est destinée au dépôt et à la diffusion de documents scientifiques de niveau recherche, publiés ou non, émanant des établissements d'enseignement et de recherche français ou étrangers, des laboratoires publics ou privés.



Distributed under a Creative Commons Attribution - NonCommercial 4.0 International License

Heat transfer enhancement of a natural convection flow in an enclosure submitted to a small extent thermal disturbance : influence of location and frequency

P. Chorin^a, F. Moreau^a, D. Saury^{a,*}

^a*Institut Pprime, UPR CNRS 3346, ISAE-ENSMA, Université de Poitiers, BP 40109 - 86961 Chasseneuil Futuroscope, France*

Abstract

A numerical study is conducted on a natural convection flow in a differentially heated cavity of aspect ratio 4, submitted to a small-extend thermal disturbance localized on the hot wall. The disturbance is a sinusoidally-varying thermal oscillation applied to the hot wall temperature on an area representing 10% of the whole hot wall. The influence of the disturbance location and frequency is investigated with the aim of acting on the flow and consequently maximizing heat transfers. The Rayleigh number is set at $Ra_H = 9 \times 10^7$ and the working fluid is air. Results show that the optimal disturbance location is at the top of the hot wall. The maximal heat transfers are obtained for two disturbance frequencies : the frequency of internal gravity waves and a very low frequency, for which the gain is higher. The disturbance is also responsible for the emergence of travelling waves and the resulting unsteady behavior of the flow is enlightened.

*. Corresponding author
Email address: didier.saury@ensma.fr (D. Saury)

Keywords. Natural convection, Differentially heated cavity, Heat transfer modification.

Nomenclature

A	aspect ratio, $A = H/L$
f	dimensionless frequency (scaled by $\alpha\sqrt{Ra_H}/H^2$)
g	gravitational acceleration, $m.s^{-2}$
H	cavity height (reference length), m
L	cavity width, m
$Nu(Z)$	local Nusselt number, $Nu(Z) = -\frac{\partial\theta}{\partial X}(Z)$
\overline{Nu}	overall Nusselt number, $\overline{Nu} = \int_0^1 Nu(Z) dZ$
$\langle Nu \rangle$	time-averaged Nusselt number, $\langle Nu \rangle = f * \int_0^{1/f} Nu(t) dt$
p_m	dimensionless driving pressure (scaled by $\rho_0 \frac{\alpha^2}{H^2} Ra_H$)
Pr	Prandtl number, $Pr = \nu/\alpha$
Ra_H	Rayleigh number based on cavity height, $Ra_H = \frac{g\beta\Delta TH^3}{\nu\alpha}$
S	stratification parameter, $S = \frac{\partial\theta}{\partial Z}(X = 0.125; Z = 0.50)$
t	dimensionless time (scaled by $H^2/(\alpha\sqrt{Ra_H})$)
T	temperature, K
T_0	mean temperature, $T_0 = \frac{1}{2}(T_h + T_c)$, K
U, W	dimensionless velocities (scaled by $\alpha\sqrt{Ra_H}/H$)
X, Z	dimensionless coordinates (scaled by H)
Z^*	adapted elevation (scaled by H)

Greek symbols

α	thermal diffusivity, $m^2.s^{-1}$
β	thermal expansion coefficient, K^{-1}
$\delta_{5\%}$	dimensionless location of the boundary layer edge
ΔT	temperature difference between the isothermal walls, $\Delta T = T_h - T_c$, K
θ	dimensionless temperature, $\theta = (T - T_0)/\Delta T$
λ	thermal conductivity, $W.m^{-1}.K^{-1}$
ν	cinematic viscosity, $m^2.s^{-1}$
ρ	density, $kg.m^{-3}$
τ	dimensionless disturbance period (scaled by $H^2/\alpha\sqrt{Ra_H}$)

Subscripts and superscripts

ad	advection
BV	Brunt-Väisälä
c	cold
cent	center of the disturbance area
d	disturbance
h	hot
mid	vertical mid-plane
ref	reference value
sc	stratified core

Abbreviations

DHC	Differentially Heated Cavity
PSD	Power Spectral Density
RB	Rayleigh-Bénard

1. Introduction

Natural convection in enclosures has been widely studied in the past decades, firstly due to its large presence in technological applications and secondly as a fundamental test case to study natural convection with well-controlled boundary conditions.

In most of previous studies, boundary conditions are generally time-independent, although for many of the corresponding applications the thermal conditions are varying over time. For example, natural convection flows induced by solar heating, such as for renewable energy production or for building ventilation, is varying over time on a daily basis [1]. Electronic devices can be periodically heated, as multi-core processors alternatively switching of jobs between its cores, which generates complex natural convection flows and heat transfers in their environment [2].

Beyond those practical examples, it is interesting to introduce a periodic thermal disturbance in order to act on heat transfers. Periodic thermal disturbances have been of interest to particular configurations of enclosures [2, 3, 4, 5, 6, 7]. Most of the time, natural convection in enclosure is generated by imposing two different temperatures on opposite walls, which creates a thermal gradient and consequently buoyancy forces. In this way, the two classical configurations mainly used to study natural convection in enclosures are the Rayleigh-Bénard (RB) configuration, where the isothermal walls are horizontal, and the Differentially Heated Cavity (DHC), where the isothermal walls are vertical. Some authors have introduced a periodic thermal oscillation in the RB configuration and have shown modifications of the flow and the associated heat transfers [8, 9, 10, 11, 12].

In the current study, the DHC configuration is considered, as this configuration is representative of many practical applications. The DHC configuration has been the subject of great interest since the pioneer work of [13]. With the development of numerical methods always more accurate, combined with calculation capacities always larger, this configuration with well-controlled boundary conditions became a classical problem for numerical simulations due to the complex coupling between velocity and temperature occurring in natural convection flows. This has led to the release of benchmark solutions for square [14] and cubic [15] cavities. Due to numerical complexity, those studies have focused on laminar steady flows. Later, some authors have developed numerical techniques to analyze the mechanisms of the transition to the unsteady flow [16, 17, 18, 19, 20]. The transition to unsteady flow in DHC has also been quantified experimentally [21]. Beyond this transition, the unsteady flows in cavity progressively degenerate into fully turbulent flows [22, 23, 24].

Once the natural convection flows in enclosures with steady boundary conditions became better understood, some authors started to implement a thermal oscillation into the cavity. [25] and [26] replaced the isothermal boundary condition on the hot wall by a pulsating heat flux. Depending on the Prandtl and Rayleigh numbers, a resonance phenomenon occurs when the frequency, matches with the period of circulation of the enclosed fluid. The resonance maximizes the fluctuations of the overall heat transfer through the vertical mid-plane. Later, Kwak et al. [1, 27] studied a square DHC with a sinusoidally time-varying temperature on the whole hot wall. As [25, 26], they observed a resonance phenomenon when the resonance frequency matches

the fundamental frequency of the internal gravity waves. A periodic flow reversal happened at this frequency, leading to an increase of the overall Nusselt number. [28] also considered a square DHC with sinusoidally-varying temperature on the whole hot wall but with an imposed frequency one order of magnitude higher than the frequency of gravity waves. The maximal gain on heat transfers was obtained when the disturbance is in tune with the frequency of Tollmien-Schlichting waves. For their part, [29] studied the influence of the aspect ratio of a DHC submitted to a sinusoidally-varying temperature on the hot wall. In comparison to the mean heat transfer without disturbance, they found that the increase of the mean heat transfer with the disturbance is higher for shallow cavities. Finally, [30] considered a cubic cavity submitted to a sinusoidally-varying hot wall temperature. As for 2D studies, a resonance was observed for large Rayleigh numbers and was determined by the amplitude and the frequency of the disturbance. 2D flows in enclosure are thus a good approximation of 3D flows.

In all these studies, the modification of thermal boundary conditions was applied on the entire hot wall. In an experimental work, [31] introduced a thin pipe with a periodically time-varying temperature localized at the bottom of the hot wall. The introduced obstacle induced a decrease of the downstream heat transfers, and the temperature oscillation of the pipe amplified the fluctuations of the unsteady flow. Recently, a localized time variation of the imposed temperature on a part of the hot wall has been studied by [32]. The disturbance area on which the temperature is varying was located at the beginning of the vertical boundary layer. The time-averaged temperature applied with thermal disturbance was either lower or higher than the hot wall

temperature. Depending on the considered case, a sinusoidal component was added with a frequency equal to the first frequency of the unsteady flow. An increase or a decrease of the overall heat transfer was obtained, depending on the time-averaged temperature of the disturbance.

For the current study, a localized disturbance is also set on the hot wall of a DHC. However, the time-averaged temperature of the disturbance is here equal to the temperature of the hot wall to avoid a heat transfer modification due to a lower or higher time-averaged disturbance temperature. The spatial extend of the disturbance is small to involve only a small modification of the DHC boundary conditions : the size of the disturbance is set at 10% of the whole length of the vertical wall. The influence of the location and the frequency of the disturbance is analyzed in terms of heat transfer modifications. Then the frequencies maximizing the overall heat transfer are studied in detail as well as the obtained unsteady flow.

2. Mathematical model

The considered DHC is a rectangular (2D) cavity with an aspect ratio $A = \frac{H}{L} = 4$, where H and L are the height and width of the cavity, respectively, with isothermal vertical walls at a temperature T_h for the hot wall and T_c for the cold wall ($\Delta T = T_h - T_c > 0$) and adiabatic horizontal walls (see Fig. 1). The flow is idealized as two-dimensional which does not affect the transition to unsteady regime [33] or the heat transfer. No-slip boundary condition $U = W = 0$ is applied on all walls, where U and W are horizontal and vertical velocity components, respectively. The working fluid is air whose thermophysical properties, except for the density, are assumed constant and

are evaluated at the mean temperature $T_0 = \frac{1}{2}(T_h + T_c) = 20^\circ C$: Prandtl number $Pr = 0.711$, conductivity $\lambda = 0.0257 W.m^{-1}.K^{-1}$ and heat capacity $C_p = 1005 J.kg^{-1}.K^{-1}$. The Boussinesq approximation is used, i.e. the density is varying only in the buoyancy term of the vertical momentum equation and is linearized against temperature :

$$\rho(T) = \rho_0 [1 - \beta(T - T_0)] \quad (1)$$

where $\rho(T)$ is the fluid density, $\rho_0 = 1.207 kg.m^{-3}$ and $\beta = 3.41 \times 10^{-3} K^{-1}$ is the thermal expansion coefficient. The Rayleigh number is based on the cavity height :

$$Ra_H = \frac{g\beta\Delta TH^3}{\nu\alpha} \quad (2)$$

The lengths, velocities, times and pressures are scaled by H , $\frac{\alpha}{H}\sqrt{Ra_H}$, $\frac{H^2}{\alpha\sqrt{Ra_H}}$ and $\rho_0\frac{\alpha^2}{H^2}Ra_H$, respectively. The dimensionless temperature is defined as $\theta = \frac{T-T_0}{\Delta T}$. Under those assumptions, the non-dimensional governing equations for mass, momentum and energy conservation are :

$$\nabla \cdot \mathbf{V} = 0 \quad (3)$$

$$\frac{\partial \mathbf{V}}{\partial t} + (\mathbf{V} \cdot \nabla) \mathbf{V} = -\nabla p_m + Pr \theta \mathbf{e}_z + \frac{Pr}{\sqrt{Ra_H}} \nabla^2 \mathbf{V} \quad (4)$$

$$\frac{\partial \theta}{\partial t} + (\mathbf{V} \cdot \nabla) \theta = \frac{1}{\sqrt{Ra_H}} \nabla^2 \theta \quad (5)$$

where \mathbf{e}_z is the upward oriented unit vector of the Z axis. The local heat transfer on isothermal walls is characterized by the Nusselt number at the elevation Z : $Nu(Z) = -\frac{\partial \theta}{\partial X}(Z)$. \overline{Nu} is the space-averaged Nusselt number over an entire wall and $\langle Nu \rangle$ is the time-averaged Nusselt number. The

relative amplitude and relative percentage gain are then defined as :

$$A_{Nu} = \frac{\max(\overline{Nu}(t)) - \min(\overline{Nu}(t))}{\langle \overline{Nu} \rangle} \quad (6)$$

$$\%G_{Nu} = 100 \frac{\langle \overline{Nu} \rangle - \langle \overline{Nu}_0 \rangle}{\langle \overline{Nu}_0 \rangle} \quad (7)$$

where $\langle \overline{Nu}_0 \rangle$ corresponds to the overall Nusselt number without disturbance (reference case). Moreover, the overall Nusselt number on the vertical mid-plane, $\langle \overline{Nu}_{mid} \rangle$, is defined as (see for instance [26]) :

$$\langle \overline{Nu}_{mid} \rangle = \int_0^1 \left(\left\langle -\frac{\partial \theta}{\partial X} + \sqrt{Ra_H Pr U \theta} \right\rangle_{X=0.125} \right) dZ \quad (8)$$

A small extent thermal disturbance is introduced on the hot wall of the cavity (see Fig. 1). On the disturbance area, a sinusoidal oscillation is added to the constant hot wall temperature :

$$\theta_d(t) = \theta_h + \sin(2\pi f_d t) \quad (9)$$

where f_d is the imposed disturbance frequency. The disturbance area is located between elevations Z_1 and Z_2 such as $Z_2 - Z_1 = 0.10$. Therefore the disturbance is localized only over 10% of the whole hot wall to introduce a limited change of the boundary conditions. The center of the disturbance area is $Z_{cent} = \frac{1}{2}(Z_1 + Z_2)$.

3. Numerical methods

All the computations have been performed using the CFD software *Code_Saturne* [34]. The discretization of the Navier-Stokes and energy equations is based on a co-located finite-volume approach on a cartesian mesh.

A conservative second-order scheme in space is applied to the momentum and energy equations. The temporal discretization is achieved with a second-order Crank-Nicholson scheme. The time step is chosen to keep the Courant–Friedrichs–Lewy number lower than one in all cells. A prediction-correction algorithm, similar to SIMPLEC, is used for pressure-velocity coupling. The mesh is non-uniform with a cell distribution in the two directions given by the density function $d(m) = \cosh(4m - 2)$, $m \in [0; 1]$, in order to refine the mesh near the walls. 130×260 control volumes are chosen following a mesh convergence study. More details and validation tests can be found in [32].

4. Results and discussion

For a vertical differentially heated cavity of aspect ratio 4, the first developing unsteadiness are boundary layer instabilities. Indeed, contrary to smaller aspect ratio cavities where the first developing unsteadiness emerge from the loss of stability at the base of the detached flow region [19], the first emerging oscillations for this aspect ratio are Tollmien-Schlichting waves travelling inside the boundary layers [20]. The strategy considered in this paper is to trigger locally flow fluctuations. That is why all the results presented hereafter are obtained for $Ra_H = 9.0 \times 10^7$, corresponding to a Rayleigh number slightly lower than the Rayleigh number at which the transition from a steady to an unsteady flow occurs, at $Ra_{H,crit} = 1.032 \times 10^8$ in 2D numerical studies [20]. Thus no fluctuations are initially present in the undisturbed flow. The influence of two parameters of the disturbance is first studied : the disturbance frequency, f_d , and the disturbance elevation, Z_{cent} .

4.1. Influence of the disturbance elevation

In order to study the influence of the disturbance elevation, the disturbance frequency is first set. Several authors have shown that the thermally stratified core of a DHC can sustain internal gravity waves, whose frequencies are lower or equal to the Brunt-Väisälä frequency, f_{BV} [20, 35]. f_{BV} is the frequency of gravity waves in an infinite stratified medium, and acts as a cut-off frequency for gravity waves in confined space. Following the previous observations of Kwak et al. [27] for a square cavity submitted to a thermal oscillation on the entire hot wall, f_d is first set at the fundamental frequency of the internal gravity waves. The frequencies of internal gravity waves modes are given by Thorpe et al. [36] :

$$f(n, p) = \frac{f_{BV}}{\sqrt{1 + \left(\frac{n}{pA_{sc}}\right)^2}} \quad (10)$$

where n and p are the numbers of half-wavelengths in the Z- and X-directions, respectively, and A_{sc} is the aspect-ratio of the stratified core. For the fundamental mode, $n = p = 1$ and for this Rayleigh number and this cavity aspect ratio, the stratified core is such as $A_{sc} > 5$. In these conditions, the fundamental frequency $f(1, 1)$ is close to f_{BV} , hence the disturbance frequency is for the moment the Brunt-Väisälä frequency. With our reference time, $f_{BV} = \frac{1}{2\pi}\sqrt{SPr}$, where S is the stratification parameter.

The influence of the disturbance elevation is studied on the whole hot wall. As the main goal of the disturbance is to enhance heat transfers, the maximum of the overall Nusselt number is the criterion to assess the best disturbance elevation. For this purpose, the percentage gain on the overall Nusselt number, $\%G_{Nu}$, versus the disturbance elevation, Z_{cent} , is plotted in Fig. 2. The error

bars correspond to the uncertainties on the calculation of the time-averaged values \overline{Nu} . Starting from the bottom of the wall, $\%G_{Nu}$ first decreases and becomes even slightly negative. Above the mid-height of the wall, $\%G_{Nu}$ becomes again positive and progressively increases up to the top of the wall. The maximal gain is 2.7% for $Z_{cent} = 0.95$, i.e. for a disturbance area between $Z = 0.90$ and the top wall. Thus this elevation is the most relevant to increase heat transfer, at the chosen frequency. Consequently, this elevation is chosen to study the influence of the disturbance frequency.

4.2. Influence of the disturbance frequency

Henceforth, the disturbance elevation is set at $Z_{cent} = 0.95$ and the influence of the disturbance frequency is now studied. The impact of the disturbance on the overall heat transfer will be first studied for three particular frequencies : a very low frequency $f_d = 0.007f_{BV}$, the fundamental frequency of internal gravity waves $f_d = f_{BV}$ and a higher frequency $f_d = 5f_{BV}$. For this purpose and as a first step, the temporal evolution of the overall Nusselt numbers at the cold and hot walls, $\overline{Nu}_c(t)$ and $\overline{Nu}_h(t)$, are plotted in Fig. 3 for these disturbance frequencies.

- For $f_d = 0.007f_{BV}$ (Fig. 3a) : $\overline{Nu}_c(t)$, $\overline{Nu}_h(t)$ and the disturbance temperature $\theta_d(t)$ are in phase. The reference velocity is $v_{ref} = \frac{\alpha}{H}\sqrt{Ra_H}$ and the reference time is $t_{ref} = \frac{H}{v_{ref}}$ (see section 2). The time for a particle to make one turn around the cavity, called here advection time, is about $\frac{2H+2L}{v_{ref}}$. Consequently the scaled advection time is $t_{ad} = 2(1+1/A) = 2.5$. This advection time must be compared to the disturbance period $1/f_d \approx 10^3$. As that time is much larger than the advection time, the flow is then quasi-steady against the disturbance. In other words, the thermal fluctuation created by

the disturbance is quickly advected to the cold wall so that the two overall Nusselt numbers remain in phase. In addition, the amplitudes of $\overline{Nu}_c(t)$ and $\overline{Nu}_h(t)$ are very close.

- For $f_d = f_{BV}$ (Fig. 3b) : $\overline{Nu}_c(t)$ and $\overline{Nu}_h(t)$ are no longer in phase. Indeed, the disturbance period $1/f_d \approx 7$ is much closer to t_{ad} which induces the observed dephasing. The amplitude of $\overline{Nu}_h(t)$ increases, whereas that of $\overline{Nu}_c(t)$ decreases in the same proportions.

- For $f_d = 5f_{BV}$ (Fig. 3c) : the amplitude of $\overline{Nu}_h(t)$ increases again, whereas no more variation is noticeable on $\overline{Nu}_c(t)$ which suggests that the fluctuations of the disturbance do not reach the opposite wall. In addition, it can be noticed that the temporal evolution of $\overline{Nu}_h(t)$ is here sinusoidal, unlike at the previous frequencies. Actually, $\overline{Nu}_h(t)$ is here modified only by the temperature oscillation from disturbance area.

The temporal evolution of the overall Nusselt number was studied for three specific frequencies. In the current paragraph, the reduced amplitudes of the overall Nusselt number, A_{Nu} , are investigated over the whole frequency domain considered from $f_d = 0.007f_{BV}$ to $f_d = 5f_{BV}$. This study is depicted in Fig. 4 for both hot and cold walls and the frequency is given relatively to f_{BV} . First of all, all the displayed values are obtained for cases with a disturbance, for which $f_d > 0$; indeed the case $f_d = 0$ would correspond to the reference case, which is steady and consequently $A_{Nu,0} = 0$. Three frequency domains can be distinguished on this figure. As previously shown in Fig. 3, for the lowest frequency $f_d = 0.007f_{BV}$, the magnitudes for the hot and cold walls are very close. For $f_d \leq 0.38f_{BV}$, A_{Nu} progressively increases with the frequency for the hot wall and decreases for the cold wall. From

$f_d = 0.38f_{BV}$ up to $f_d = f_{BV}$, A_{Nu} is quite constant for both walls whatever the value of f_d . For f_d higher than f_{BV} , the reduced amplitude for the hot wall increases continuously up to the maximal tested frequency $f_d = 5f_{BV}$. For the cold wall, A_{Nu} starts to decrease symmetrically compared to the evolution for the hot wall and finally tends towards zero for $f_d > 3f_{BV}$.

Thus, the phase and the amplitude of the overall Nusselt numbers are sensitive to the disturbance frequency. The influence of this parameter on the overall Nusselt numbers will be investigated here. For this purpose, $\langle \overline{Nu} \rangle$ versus the relative frequency f_d/f_{BV} is plotted in Fig. 5(a). The corresponding percentage gain relatively to the reference case is plotted in Fig. 5(b) where the frequency is in logarithmic scale. The three frequency domains previously defined are also noticeable here, with an additional fourth frequency domain for highest frequencies. Indeed, for $f_d \geq 4f_{BV}$, $\langle \overline{Nu} \rangle$ is quite constant and close to the value in the reference case ($\%G_{Nu}$ is close to 0, as seen on Fig. 5(b)). When f_d decreases up to f_{BV} , $\langle \overline{Nu} \rangle$ increases. For $f_d = f_{BV}$, $\langle \overline{Nu} \rangle$ and $\%G_{Nu}$ reach a local maximum value. Thus, a resonance phenomenon arises at the fundamental frequency of internal gravity waves. The same observation was done by [27] for an overall disturbance in a square cavity. This result shows that the resonance occurs also for a small-extend disturbance in a DHC of aspect ratio 4. From $f_d = f_{BV}$, $\langle \overline{Nu} \rangle$ and $\%G_{Nu}$ decrease with the decrease of the frequency up to $f_d = 0.38f_{BV}$, and then increase again. The values at very low frequencies exceed the values obtained at the resonant frequency $f_d = f_{BV}$. Moreover, those values seem to saturate when f_d tends towards zero. To our knowledge, these larger values for very low frequencies have not been previously observed in the literature.

For the resonant frequency $f_d = f_{BV}$ and the lowest studied frequency $f_d = 0.007f_{BV}$, denoted thereafter by $f_d \ll f_{BV}$, the gain on overall Nusselt number reach local maxima equal to 2.74% and 3.88%, respectively. Therefore a focus is done henceforth on those two particular frequencies. It can be noted that if Ra is reduced to 5.0×10^7 or increased to 1.5×10^8 , the gains on Nusselt numbers for $f_d = f_{BV}$ (2.58% and 2.78%) and for $f_d \ll f_{BV}$ (3.69% and 3.92%) are very close to the values obtained at the tested Rayleigh number 9.0×10^7 . Moreover, the optimal disturbance elevation for $f_d = f_{BV}$ has been found throughout the study of the influence of Z_{cent} for this frequency (see Fig. 2). In order to check if this elevation is also optimal for the low frequency, Table 1 gathers the gains of $\langle \overline{Nu} \rangle$ for several values of Z_{cent} . As shown, the optimal elevation for the low frequency is also at the top of the hot wall ($Z_{cent} = 0.95$). Consequently, this elevation is still selected for the study at the two frequencies of maximal gains.

4.3. Study at the frequencies of maximal gains

As previously explained, the overall heat transfers are maximal for $f_d \ll f_{BV}$ and $f_d = f_{BV}$. In order to see how those heat transfer increases are distributed along vertical walls for both frequencies, local Nusselt numbers along the adapted elevation Z^* are plotted in Fig. 6. The adapted elevation Z^* corresponds to Z on the hot wall and to $1 - Z$ on the cold wall. This takes advantage of the centrosymmetry property of the flow in the reference case, resulting in an overlap of $\langle Nu_{h,ref}(Z) \rangle$ and $\langle Nu_{c,ref}(1 - Z) \rangle$. However, with the disturbance introduced on the hot wall, the flow is no more centrosymmetric. It can be seen on Fig. 6(a) that $\langle Nu_h(Z) \rangle$ is strongly modified in the disturbance area ($0.9 < Z < 1$). For $0.90 \leq Z \leq 0.96$ (Area 2), $\langle Nu_h(Z) \rangle$

is larger than the corresponding value in the reference case : the local Nusselt number, first, increases considerably at the beginning of the disturbance area and then decreases almost linearly downstream. For $Z > 0.96$ (Area 1), $\langle Nu_h(Z) \rangle$ keeps decreasing, becomes even negative and finally reaches $\langle Nu_h(Z = 1) \rangle = -5$. The increase on Area 2 is larger than the decrease on Area 1, and as the obtained profile along the rest of the wall is very close to the one of the reference case, that leads to the increase of the overall heat transfer previously mentioned. On the cold wall, the modification of local Nusselt number is limited to $Z > 0.90$ ($Z^* < 0.10$, Area 3). This area is located in front of the disturbance area and corresponds to the part of the cold wall reached by the impinging flow coming from the hot wall. The surface of Area 3 is equal to the difference between the surfaces of Area 2 and Area 1 to ensure energy conservation. On Fig. 6(b), it can be noticed that the reduction of $\langle Nu_h(Z) \rangle$ at the top of the hot wall is less pronounced for $f_d \ll f_{BV}$ than for $f_d = f_{BV}$ (Area 4). Moreover, for the same Z^* locations, an increase of $\langle Nu_c(Z^*) \rangle$ is observed on the cold wall (Area 5). Thus, the increase for $f_d = f_{BV}$ noticed on the Area 3 has extended up to $Z = 0.80$ ($Z^* = 0.20$) for the disturbance at the low frequency. Those local increases on Area 4 and Area 5 cause the higher heat transfer at the low frequency compared to the one at the Brunt-Väsälä frequency.

Those modifications on local heat transfers are related to modifications of the temperature distribution inside the cavity. For this purpose, time-averaged temperature fields for the reference case and for the two considered frequencies are given in Fig. 7. In the reference case, the temperature field is centrosymmetric about the center of the cavity. However, for both frequen-

cies, a region where the time-averaged temperature, $\langle \theta \rangle$, is higher than 0.5 can be seen at the top of the cavity. That means that the temperature in this region, averaged over a period of disturbance, is higher than the hot wall temperature θ_h , even while the time-averaged temperature of the disturbance is equal to θ_h . This has been also observed by [1] in a square cavity submitted to a disturbance applied on the entire wall. The temperature deviation with respect to the reference case expresses the non-linear effects introduced by the disturbance. Indeed, the overheating below the top wall causes simultaneously the negative value of $\langle Nu_h(Z) \rangle$ for $Z > 0.96$ and the increase of $\langle Nu_f(Z) \rangle$ at the upper part of the cold wall depicted in Fig. 6.

The relative gains obtained on time-averaged heat transfers have been analyzed in terms of local heat transfer modifications and time-averaged temperature fields. As the introduced disturbance is time-varying, a temporal variation of the temperature of the flow is expected, which causes the temporal evolution of the overall Nusselt numbers previously discussed. In order to determine which frequencies appear in this unsteady flows, Power Spectral Densities (PSD) of temperature signals recorded at the center of the cavity ($X = 0.125 ; Z = 0.50$) and at the end of the cold boundary layer ($X = 0.21 ; Z = 0.10$) for both disturbance frequencies are plotted in Fig. 8. $2^{11} = 2048$ and $2^{19} = 524288$ measurement points are recorded for $f_d = f_{BV}$ and $f_d \ll f_{BV}$, respectively, allowing to obtain sufficient frequency resolutions. In order to improve the quality of the signal, the displayed spectra are obtained by averaging 2 spectra for Fig. 8(a,b,c), and 32 spectra for Fig. 8(d).

For $f_d = f_{BV}$, at the two considered locations (Fig. 8(a,b)), the fundamental

frequency is the disturbance frequency, and numerous harmonics are observed in the PSD (only the first seven harmonics are displayed). Those harmonics show that the initial thermal fluctuation created by the disturbance is strongly modified by the flow. In addition, as seen on Fig. 8(b), the fluctuations generated at the disturbance area are spread by the main flow and the stratified core is excited by gravity waves, as seen on Fig. 8(a). This leads the resonance phenomenon observed on Fig. 5, as the stratified core resonates at the internal gravity wave frequency.

For $f_d \ll f_{BV}$ at the center of the cavity (Fig. 8(c)), the PSD is much more complex and displays a lot of peaks concentrated in two spectral domains. The first spectral domain is for f lower than f_{BV} or close to it. The corresponding frequencies are associated to internal gravity waves (Eq. 10). Thus, as for $f_d = f_{BV}$, the internal gravity waves are excited by the introduction of the low-frequency disturbance. The second spectral domain appears for $f \in [0.35 ; 0.60]$, where peaks are gathered in six main sets. Each set corresponds to one of the six unsteady modes successively emerging in a differentially heated cavity with the current aspect ratio [20]. Those modes are associated to Tollmien-Schlichting waves travelling along the vertical boundary layers when such a flow becomes unsteady. Consequently, they are amplified inside the boundary layers, as seen at the end of the cold boundary layer on Fig. 8(d). At that location, the amplitudes of Tollmien-Schlichting waves are higher than the amplitudes of internal gravity waves : Tollmien-Schlichting waves are here predominant. The mechanisms of the transition to unsteady flow seems to be also triggered by the low-frequency disturbance. Indeed, the emergence of Tollmien-Schlichting waves is here facilitated since the conside-

red Rayleigh number is close to the critical Rayleigh number beyond which Tollmien-Schlichting waves appear.

Those frequencies detected inside the cavity are related to a time evolution of the flow. In order to visualize this evolution, temperature fluctuations for four snapshots over a period of disturbance, τ , are displayed in Fig. 9. The temperature fluctuations are given by $\theta' = \theta - \langle \theta \rangle$. A particular focus is made on the lower half of the cavity as the waves are more developed in this area.

The edge of the cold boundary layer is also displayed from $Z = 0.5$ to $Z = 0.2$ (below $Z = 0.2$ the boundary layer can not be defined). The location of the edge is given by $\delta_{5\%}$ such as, for a given Z :

$$W(X = \delta_{5\%}(Z)) = 0.05 \min[W(X)]$$

For $f_d \ll f_{BV}$ on Fig. 9 (bottom), a large structure with positive and negative temperature fluctuations can be seen in the top part of the displayed fields at $t = t_0 + \tau/4$ and $t = t_0 + 3\tau/4$, respectively. Those temperature fluctuations are in phase with the thermal disturbance signal. It can be noted that for the two studied frequencies small lobes of local temperature fluctuations are spread inside the cold boundary layer and in the vicinity of the bottom wall. For $f_d = f_{BV}$ (Fig. 9 top), the lobes are present during the whole disturbance cycle. They are related to the propagation of the disturbance, in accordance with the spectrum on Fig. 8 (b), as the main frequency is the disturbance frequency. For $f_d \ll f_{BV}$, the lobes are observed only between $t = t_0 + 3\tau/4$ and $t = t_0 + \tau$. At this frequency, the thermal lobes are related

to Tollmien-Schlichting waves, as seen in the spectral analysis on Fig. 8 (d), which are travelling inside the cold boundary layer. These travelling waves are usually formed when Ra_H is higher than the critical Rayleigh number of the transition to unsteady flow [20]. Thus, the disturbance at the low disturbance frequency triggers the development of Tollmien-Schlichting waves during a part of the disturbance cycle.

5. Conclusions

A natural convection flow in a two-dimensional differentially heated cavity of aspect ratio 4 is submitted to a small-extend thermal disturbance localized on the hot wall. On the disturbance area, which represents 10% of the entire wall, a periodic component is added on the imposed hot wall temperature. The influence of the location and frequency of the disturbance is studied mainly in terms of heat transfer modifications. The aim of the disturbance is to maximize the overall heat transfer without change on the time-averaged temperature on the walls.

Firstly, the following conclusions may be drawn :

- the best location to maximize the heat transfers is located at the very top of the hot wall.
- the increase of the disturbance frequency induces an increase of the amplitude of the instantaneous heat transfer for the hot wall and a decreases towards zero for the cold wall.
- the maximal increases of the time-averaged heat transfer are obtained for two frequencies : for the fundamental frequency of internal gravity waves, previously denoted in the literature for an overall disturbance

in a square cavity, and for a very low frequency, inducing a higher heat transfer increase equal to 3.88%.

- those heat transfer increases are induced by the persistence of an over-temperature region beneath the top wall, increasing heat transfers at the top of the cold wall, and strongly modifying heat transfers at the top of the hot wall.

Secondly, as the thermal disturbance is time-dependant, it induces a temporal evolution of the flow. A detailed analysis of emerging frequencies and temperature fluctuations reveals that :

- the disturbance produces travelling waves advected by the main flow, observed in the cold boundary layer and near the bottom wall.
- a spectral analysis reveals that for the disturbance at the frequency of internal gravity waves, only the fundamental frequency of those waves and the corresponding harmonics are detected in the flow. However, for the very low frequency, Tollmien-Schlichting waves are detected in addition to gravity waves ; Tollmien-Schlichting waves are usually observed in the unsteady regime beyond the current Rayleigh number. Consequently the disturbance at this frequency triggers the unsteady flow regime.

Those results show the capability of a well-positioned small-extend disturbance, which requires only a local modification of the enclosure, to enhance the overall heat transfer. Moreover, an oscillation at very low frequency can involve a complex unsteady behavior of the flow. It could be interesting, for

future studies, to investigate the influence of such disturbance on cavities of other aspect ratios and to change the Prandtl number of the working fluid.

6. Acknowledgments

The authors would thank the CPER (2015-2020) and the ERDF (2014-2020) grants for supporting this work.

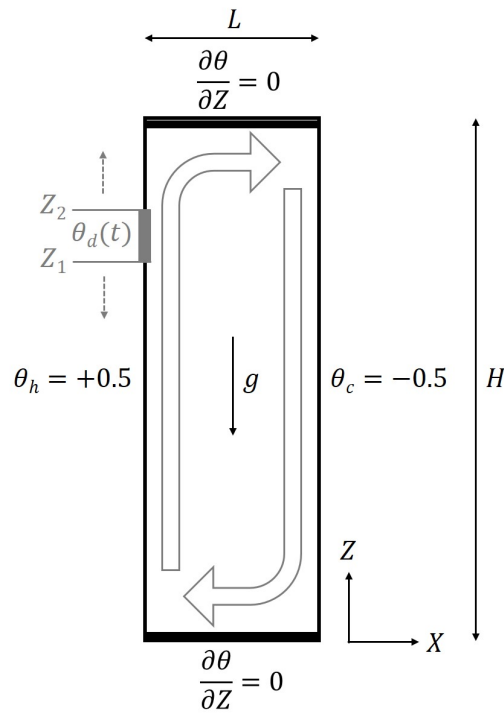


FIGURE 1: Scheme of the differentially heated cavity with a disturbance area located between Z_1 and Z_2 .

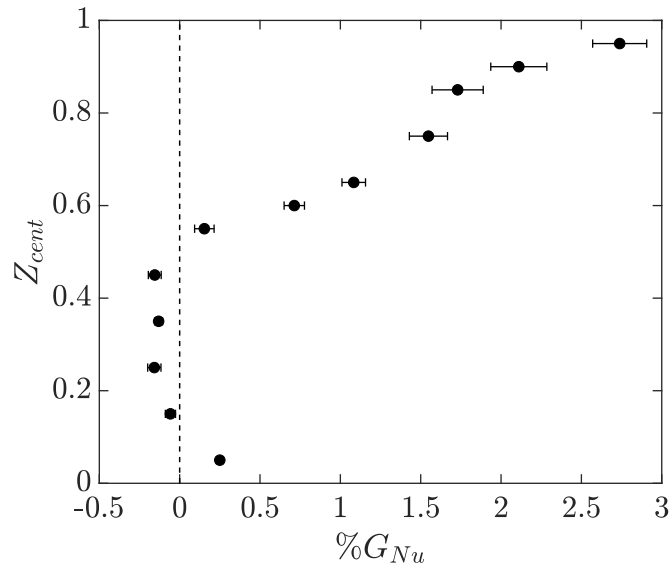


FIGURE 2: Gain on average Nusselt number, $\%G_{Nu}$, versus the elevation of the disturbance, Z_{cent} , for $f_d = f_{BV}$.

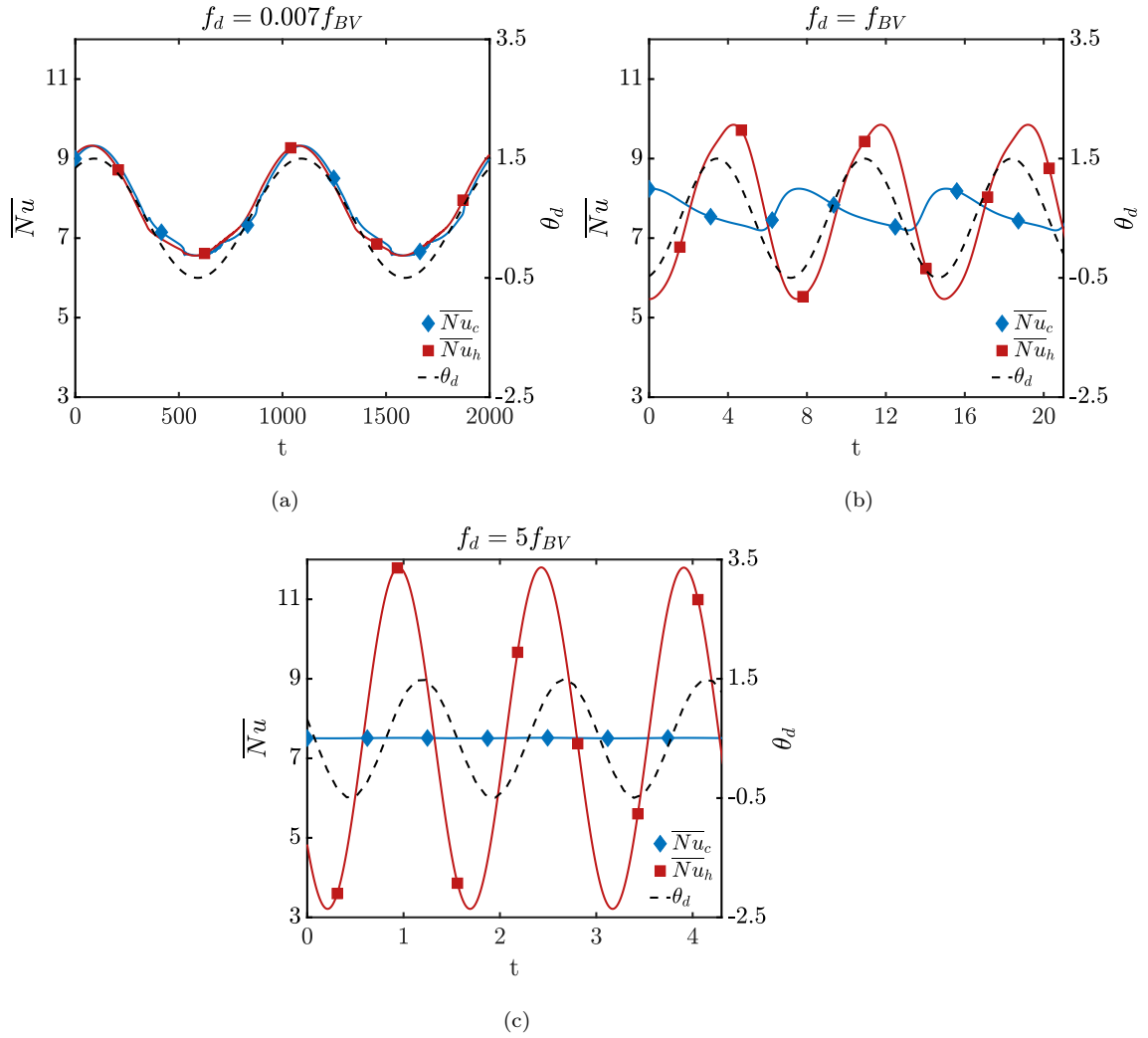


FIGURE 3: Temporal evolution of instantaneous Nusselt numbers on the cold and hot walls for different disturbance frequencies; the instantaneous temperature of the disturbance, $\theta_d(t)$, is overprinted.

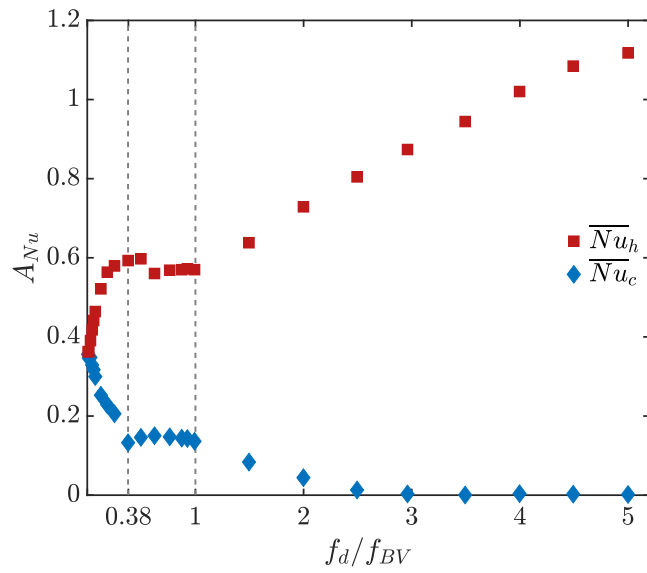


FIGURE 4: Temporal amplitude of the instantaneous Nusselt number, A_{Nu} , versus the reduced disturbance frequency, f_d/f_{BV} , for the hot and cold walls.

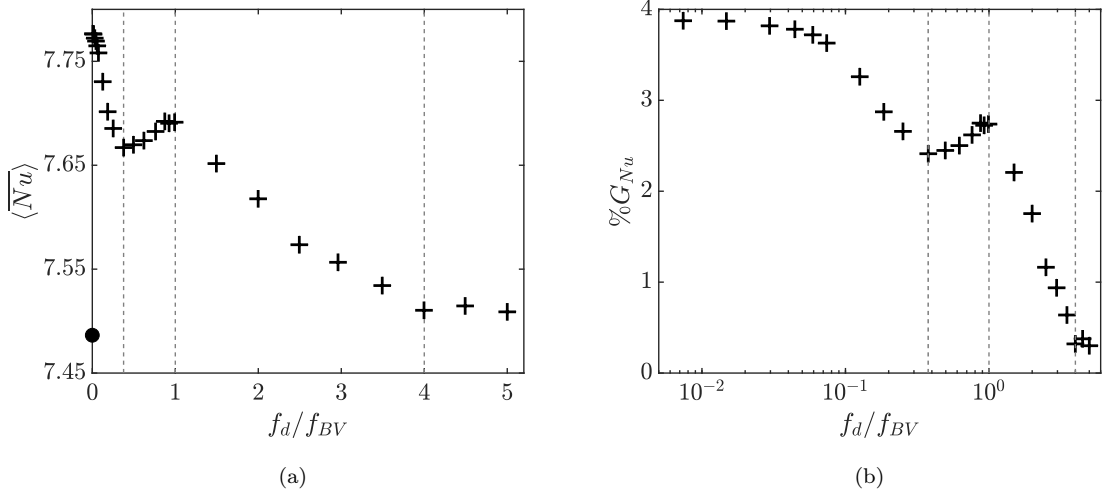
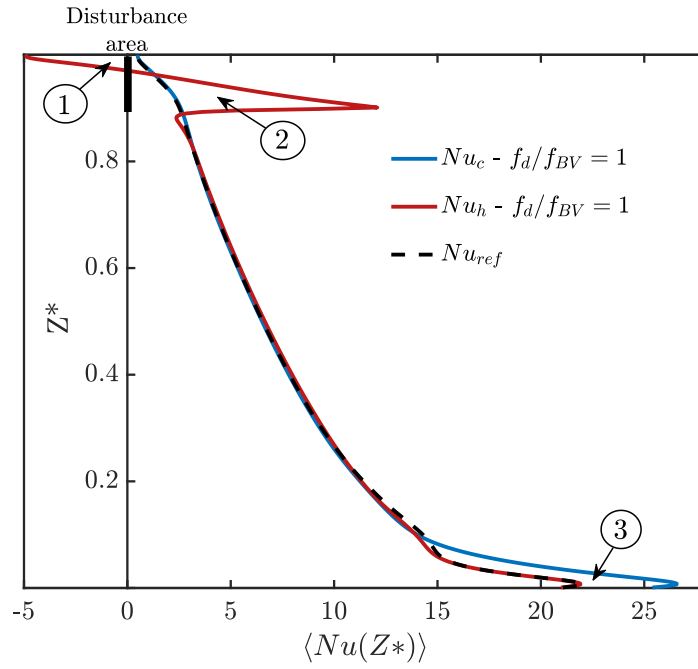


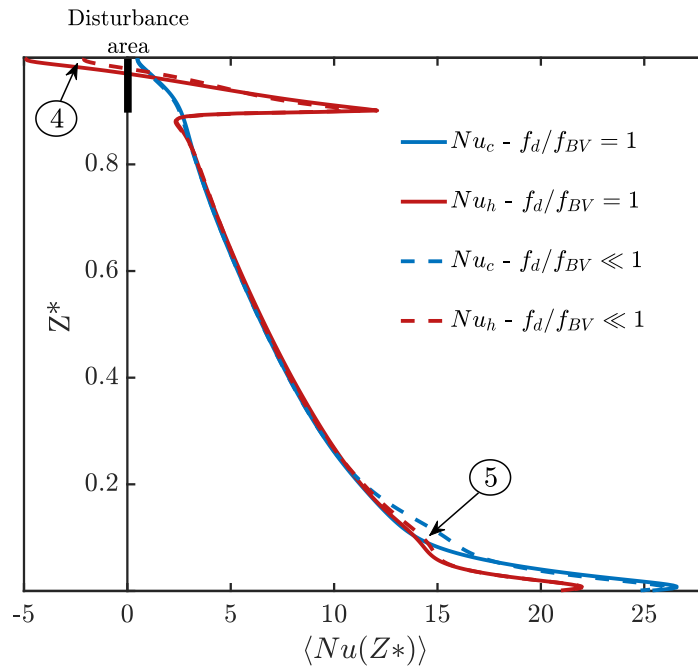
FIGURE 5: (a) Time-averaged overall Nusselt number, $\langle \overline{Nu} \rangle$, versus the disturbance frequency; the Nusselt number without disturbance is represented by a point on the vertical axis; (b) gain (percentage) on time-averaged overall Nusselt number, $\%G_{Nu}$, versus the disturbance frequency.

Z_{cent}	0.25	0.55	0.85	0.90	0.95
$\%G_{Nu}$	0.18	0.50	1.40	2.28	3.88

TABLE 1: Gains (percentage) on overall Nusselt numbers, $\%G_{Nu}$, for several locations of the center of the disturbance area, Z_{cent} , for $f_p/f_{BV} \ll 1$.



(a)



(b)

FIGURE 6: Time-averaged local Nusselt number, $\langle Nu(Z^*) \rangle$, versus adapted elevation Z^* : $Z^* = Z$ on the hot wall, $Z^* = 1 - Z$ on the cold wall; (a) without disturbance (reference case) and for $f_d = f_{BV}$; (b) for $f_d = f_{BV}$ and for $f_d \ll f_{BV}$.

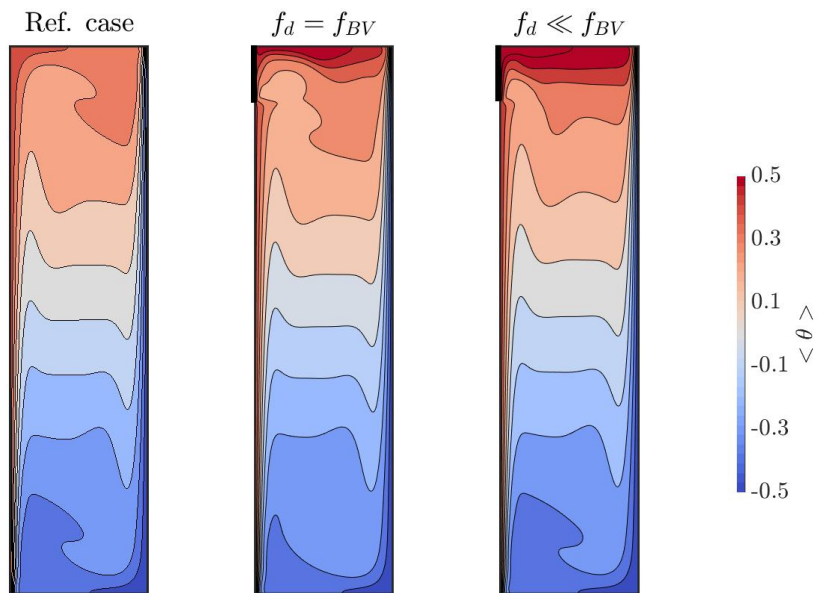


FIGURE 7: Time-averaged temperature field for the reference case and for the two frequencies of maximal heat transfer, $\Delta\theta = 0.1$; the disturbance area is displayed (top left of the cavity).

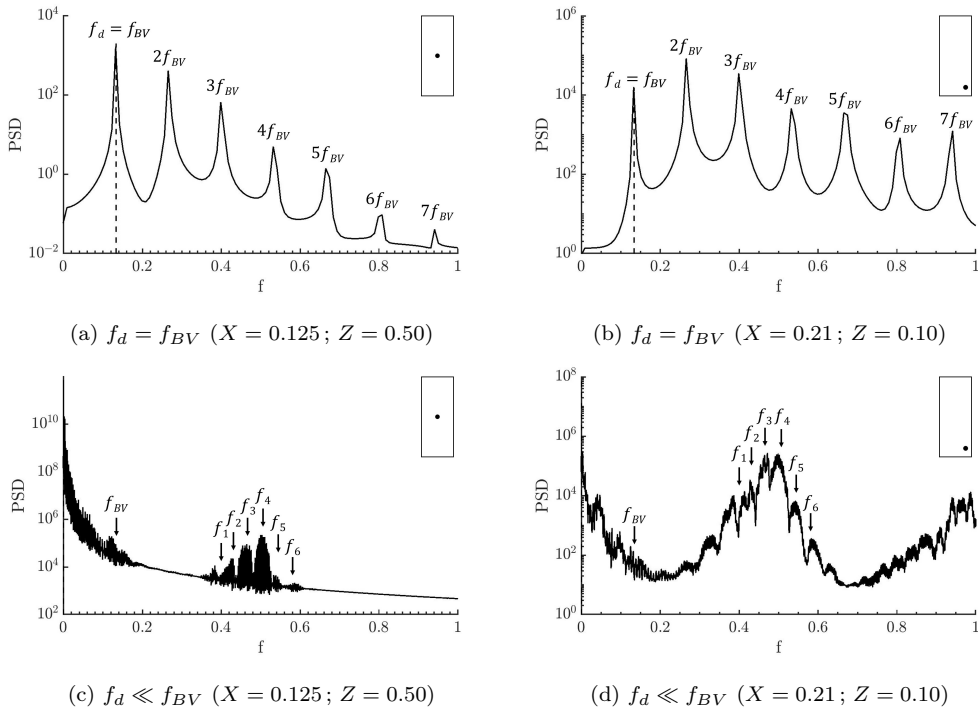


FIGURE 8: Power Spectral Density on instantaneous temperature for $f_d = f_{BV}$ and $f_d \ll f_{BV}$, at $(X = 0.125; Z = 0.50)$ and $(X = 0.21; Z = 0.10)$; for each case the measurement location is inserted.

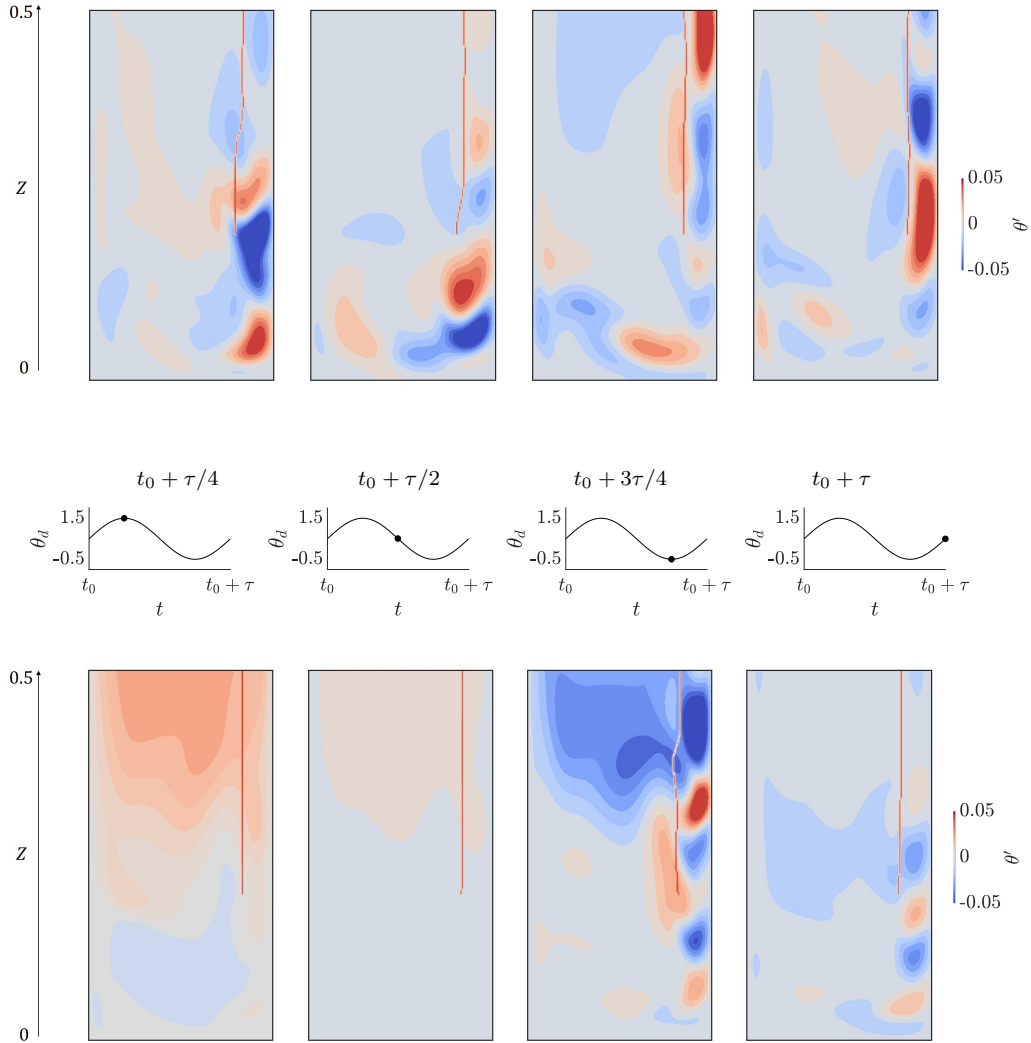


FIGURE 9: Fluctuation of temperature, $\theta' = \theta - \langle \theta \rangle$, in the lower half of the cavity for four instants equally distributed in a period τ ; (top) $f_d = f_{BV}$ (bottom) $f_d \ll f_{BV}$; the edge of the cold boundary layer, $\delta_{5\%}$, is overprinted. For each snapshot the instantaneous temperature of the disturbance during its cycle is plotted.

Références

- [1] H. Kwak, K. Kuwahara, and J. Hyun, “Resonant enhancement of natural convection heat transfer in a square enclosure,” *International Journal of Heat and Mass Transfer*, vol. 41, pp. 2837–2846, SEP 1998.
- [2] P. S. Mahapatra, N. K. Manna, K. Ghosh, and A. Mukhopadhyay, “Heat transfer assessment of an alternately active bi-heater undergoing transient natural convection,” *International Journal of Heat and Mass Transfer*, vol. 83, pp. 450–464, Apr. 2015.
- [3] Y. Shu, B. Li, and B. Ramaprian, “Convection in modulated thermal gradients and gravity : experimental measurements and numerical simulations,” *International Journal of Heat and Mass Transfer*, vol. 48, no. 1, pp. 145–160, 2005.
- [4] B. Ghasemi and S. Aminossadati, “Periodic natural convection in a nanofluid-filled enclosure with oscillating heat flux,” *International Journal of Thermal Sciences*, vol. 49, no. 1, pp. 1–9, 2010.
- [5] W. Zhang, C. Zhang, and G. Xi, “Conjugate conduction-natural convection in an enclosure with time-periodic sidewall temperature and inclination,” *International Journal of Heat and Fluid Flow*, vol. 32, no. 1, pp. 52–64, 2011.
- [6] P. S. Mahapatra, S. Chatterjee, A. Mukhopadhyay, N. K. Manna, and K. Ghosh, “Proper orthogonal decomposition of thermally-induced flow structure in an enclosure with alternately active localized heat sources,”

- International Journal of Heat and Mass Transfer*, vol. 94, pp. 373–379, Mar. 2016.
- [7] I. Pishkar, B. Ghasemi, A. Raisi, and S. M. Aminossadati, “Numerical study of unsteady natural convection heat transfer of newtonian and non-newtonian fluids in a square enclosure under oscillating heat flux,” *Journal of Thermal Analysis and Calorimetry*, vol. 138, no. 2, pp. 1697–1710, 2019.
- [8] L. Howle, “Control of Rayleigh-Bénard convection in a small aspect ratio container,” *International Journal of Heat and Mass Transfer*, vol. 40, pp. 817–822, MAR 1997.
- [9] B. Abourida, M. Hasnaoui, and S. Douamna, “Transient natural convection in a square enclosure with horizontal walls submitted to periodic temperatures,” *Numerical Heat Transfer A*, vol. 36, pp. 737–750, Nov. 1999.
- [10] A. Raji, M. Hasnaoui, M. Firdaouss, and C. Ouardi, “Natural convection heat transfer enhancement in a square cavity periodically cooled from above,” *Numerical Heat Transfer, Part A : Applications*, vol. 63, no. 7, pp. 511–533, 2013.
- [11] M. Z. Hossain and J. M. Floryan, “Natural convection in a fluid layer periodically heated from above,” *Physical Review E*, vol. 90, p. 023015, Aug. 2014.
- [12] M. Z. Hossain and J. M. Floryan, “Natural convection in a horizontal

- fluid layer periodically heated from above and below,” *Physical Review E*, vol. 92, p. 023015, Aug. 2015.
- [13] G. K. Batchelor, “Heat transfer by free convection across a closed cavity between vertical boundaries at different temperatures,” *Quarterly of Applied Mathematics*, vol. 12, no. 3, pp. 209–233, 1954.
- [14] G. De Vahl Davis and I. P. Jones, “Natural convection in a square cavity : A comparison exercise,” *International Journal of Numerical Methods in Fluids*, vol. 3, no. 3, pp. 227–248, 1983.
- [15] E. Tric, G. Labrosse, and M. Betrouni, “A first incursion into the 3D structure of natural convection of air in a differentially heated cubic cavity, from accurate numerical solutions,” *International Journal of Heat and Mass Transfer*, vol. 43, pp. 4043–4056, NOV 2000.
- [16] S. Paolucci and D. Chenoweth, “Transition to chaos in a differentially heated vertical cavity,” *Journal of Fluid Mechanics*, vol. 201, pp. 379–410, APR 1989.
- [17] S. Armfield and J. C. Patterson, “Direct simulation of wave interactions in unsteady natural convection in a cavity,” *International Journal of Heat and Mass Transfer*, vol. 34, no. 4-5, pp. 929–940, 1991.
- [18] E. Gadoin, P. Le Quéré, and O. Daube, “A general methodology for investigating flow instabilities in complex geometries : application to natural convection in enclosures,” *International Journal for Numerical Methods in Fluids*, vol. 37, pp. 175–208, SEP 30 2001.

- [19] P. Le Quéré and M. Behnia, “From onset of unsteadiness to chaos in a differentially heated square cavity,” *Journal of Fluid Mechanics*, vol. 359, pp. 81–107, 1998.
- [20] S. Xin and P. Le Quéré, “Natural-convection flows in air-filled, differentially heated cavities with adiabatic horizontal walls,” *Numerical Heat Transfer A*, vol. 50, pp. 437–466, SEP 15 2006.
- [21] V. Kishor, S. Singh, and A. Srivastava, “On the identification of flow instabilities in a differentially-heated closed cavity : Non-intrusive measurements,” *International Journal of Heat and Mass Transfer*, vol. 147, p. 118933, 2020.
- [22] F. Trias, A. Gorobets, M. Soria, and A. Oliva, “Direct numerical simulation of a differentially heated cavity of aspect ratio 4 with rayleigh numbers up to 10^{11} —part i : Numerical methods and time-averaged flow,” *International Journal of Heat and Mass Transfer*, vol. 53, no. 4, pp. 665–673, 2010.
- [23] F. Trias, A. Gorobets, M. Soria, and A. Oliva, “Direct numerical simulation of a differentially heated cavity of aspect ratio 4 with rayleigh numbers up to 10^{11} —part ii : Heat transfer and flow dynamics,” *International Journal of Heat and Mass Transfer*, vol. 53, no. 4, pp. 674–683, 2010.
- [24] F. Sebilliau, R. Issa, S. Lardeau, and S. P. Walker, “Direct numerical simulation of an air-filled differentially heated square cavity with rayleigh

- numbers up to 10^{11} ,” *International Journal of Heat and Mass Transfer*, vol. 123, pp. 297–319, 2018.
- [25] J. Lage and A. Bejan, “The resonance of natural convection in an enclosure heated periodically from the side,” *International Journal of Heat and Mass Transfer*, vol. 36, no. 8, pp. 2027–2038, 1993.
- [26] B. Antohe and J. Lage, “A dynamic thermal insulator : inducing resonance within a fluid saturated porous medium enclosure heated periodically from the side,” *International Journal of Heat and Mass Transfer*, vol. 37, no. 5, pp. 771–782, 1994.
- [27] H. S. Kwak and J. M. Hyun, “Natural convection in an enclosure having a vertical sidewall with time-varying temperature,” *Journal of Fluid Mechanics*, vol. 329, pp. 65–88, 1996.
- [28] S. K. Kim, S. Y. Kim, and Y. D. Choi, “Amplification of boundary layer instability by hot wall thermal oscillation in a side heated cavity,” *Physics of Fluids*, vol. 17, no. 1, p. 014103, 2005.
- [29] N. B. Cheikh, B. B. Beya, and T. Lili, “Aspect ratio effect on natural convection flow in a cavity submitted to a periodical temperature boundary,” *Journal of Heat Transfer*, vol. 129, no. 8, pp. 1060–1068, 2007.
- [30] Z. Huang, W. Zhang, and G. Xi, “Natural convection heat transfer in a cubic cavity submitted to time-periodic sidewall temperature,” *Numerical Heat Transfer A*, vol. 67, no. 1, pp. 13–32, 2015.
- [31] F. Penot, O. Skurtys, and D. Saury, “Preliminary experiments on the

- control of natural convection in differentially-heated cavities,” *International Journal of Thermal Sciences*, vol. 49, pp. 1911–1919, OCT 2010.
- [32] P. Chorin, F. Moreau, and D. Saury, “Heat transfer modification induced by a localized thermal disturbance in a differentially-heated cavity,” *International Journal of Thermal Sciences*, vol. 125, pp. 101–110, Mar. 2018.
- [33] S. Xin and P. Le Quéré, “Stability of two-dimensional (2D) natural convection flows in air-filled differentially heated cavities : 2D/3D disturbances,” *Fluid Dynamics Research*, vol. 44, no. 3, p. 031419, 2012.
- [34] F. Archambeau, N. Méchitoua, and M. Sakiz, “Code saturne : A finite volume code for the computation of turbulent incompressible flows-industrial applications,” *International Journal of Finite Volumes*, vol. 1, no. 1, pp. <https://www.code-saturne.org/cms/>, 2004.
- [35] J. Patterson and J. Imberger, “Unsteady natural convection in a rectangular cavity,” *Journal of Fluid Mechanics*, vol. 100, no. 1, pp. 65–86, 1980.
- [36] S. A. Thorpe, “On standing internal gravity waves of finite amplitude,” *Journal of Fluid Mechanics*, vol. 32, no. 3, pp. 489–528, 1968.